Development of efficient models of Magnetic Braking Systems of railway vehicles

Development of efficient models of magnetic braking systems of railway vehicles

E. Galardi, E. Meli, D. Nocciolini, L. Pugi and A. Rindi

Department of Industrial Engineering, University of Florence, via S. Marta n. 3, 50139 Firenze, Italy

Received 1 October 2014; accepted 12 January 2015

In modern railway vehicles the use of Magnetic Braking Systems is continuously increasing, because they are characterized by high braking performances and low energy consumptions. Hence, the study and the accurate modelling of Magnetic Braking Systems is a very important issue, because they significantly affect the dynamics of vehicle and electrical supply circuit. Usually the performances of Magnetic Braking Systems are evaluated on test-rigs in order to reduce times and costs of testing phases. For this reason, the authors focus on the development of a complete 3D model of Magnetic Brake System test-rig, (built in COMSOL) including all the electro-magnetic, circuital and mechanical parts. These parts are often studied separately in the literature; however a combined analysis is crucial to correctly describe the behaviour of the whole system. The proposed model is highly modular (to describe different Magnetic Brake System test-rig layouts characterized by a different number of magnetic polar expansions) and aims at obtaining a compromise between accuracy and numerical efficiency. Subsequently, a second simplified lumped parameter model derived from the complete one and built in *MATLAB* is developed, to further reduce the computational load without decreasing the results accuracy. In this work, both the models have been developed and validated in collaboration *Ferrovie dello Stato* and compared with other simplified models present in the literature.

Keywords: magnetic braking systems; railway braking; railway vehicles

Nomenclature

A	surface
$\underline{B}$	magnetic induction
$\underline{F}^{acc}$, $\underline{F}^{lump}$, $\underline{F}^{id}$, $\underline{F}^{meas}$	complete model, lumped parameter model, ideal and measured forces
$\underline{H}$	magnetic field
$\underline{J}$	current density
$L^{lump}(x)$, $L^{id}(x)$	lumped parameter model and ideal inductances
$\underline{M}^{acc}$, $\underline{M}^{lump}$	complete model and lumped parameter model moments
N	number of turns
$\underline{O}_1$	center of mass of the single polar expansion
$\underline{O}_2$	center of mass of the rail fraction
$\underline{P}_c$	contact point position
R	resistance
S	wire section
U	magnetic energy
V	voltage

*Corresponding author. Email: enrico.meli@unifi.it

i	current
n	polar expansion number
$\underline{r}$	distance
$\underline{x}$	position
$\underline{\dot{x}}$	velocity
Δt	time integration step
ε	counter electromotive force
Φ	magnetic flow
μ	permeability

1. Introduction

Magnetic Braking Systems are widely used in the railway and tramway fields because they can strongly improve the efficiency and safety of railway vehicle braking [1].

The Magnetic Brake System directly acts on the rails and is therefore independent from the wheel-rail adhesion. Its action is obtained by friction due to the magnetic attractive force generated electrically or by permanent magnets [2]. The Magnetic Brake System is installed into the bogie or running gear between the wheels to complement the braking action depending on the wheel-rail adhesion [3].

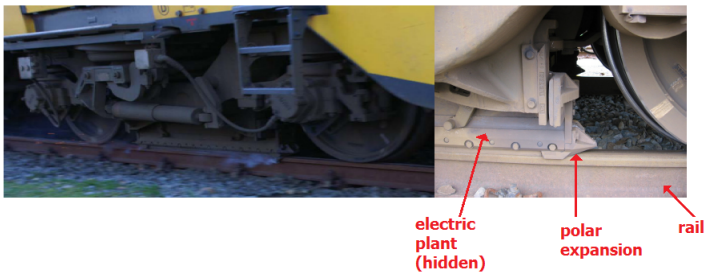

Figure 1. Typical layout of a magnetic braking system.

Moreover, Magnetic Brake System performance is a safety relevant issue in railway practice, impacting vehicle longitudinal dynamics, signaling, and traffic management, and its features and requirements are important also for interoperability problems [4]. The availability of software tools aimed at simulating the performance of Magnetic Braking Systems is useful to speed up and optimize the design process [5]. Some examples of train Magnetic Braking Systems simulators are available in the literature. In [6], David et al. presented a software tool for the evaluation of train stopping distance, developed in C language. In [7], the software TrainDy was presented; it was developed to reliably evaluate the longitudinal force distribution along a train during different operations. In [8], Kang described a Hardware In the Loop (HIL) system for the Magnetic Braking Systems of the Korean high-speed trains and analyzed the characteristics of the braking systems via Real Time (RT) simulations. In [9], many interrelationships between various factors and types of braking techniques were analyzed.

The development of accurate Magnetic Brake System mathematical models is critical and allows an accurate evaluation of the whole system behaviour (both in the design and in the operating phases) and a further improvement of the braking performances.

The results of a 2D Magnetic Brake System analytical model were compared to the normal reaction force and magnetic density provided by a complete FEM model and validated according to force experimental measurements by J.D.Edwards et al. [10], in which the effects of the brake geometric parameters are pointed out. In [11], a 3D model developed in *ANSOFT* (a software for 3D electromagnetic field simulation) was employed for the evaluation of the influencing factors of braking force on the Magnetic Brake System system.

The above mentioned papers consider complex models that couple electromagnetism with dynamics, however result in an excessive computational load, thence the coupling of these models in complete railway systems is impracticable.

In addition, many lumped parameter models can be found in literature. For instance, in [12], a 2D analytical model of a permanent magnet Eddy-current brake is presented; then, a physical analysis and a comparison with a 3D FEM model of the same component are performed. Also, Baran [13], Hazry et al.[14] presented several formulas for the computation of the braking force, derived from an Eddy-current braking system, according to its magnetic field profile. In [15], a solenoid (magnetic) valve system is modelled, for brakes employed in the automotive industry; in particular, the lumped parameter modelling of the electrical, electromechanical and mechanical subsystems is shown. Moreover, the motional Eddy-currents modelling is achieved through the Magnetic Equivalent Circuits (MEC) method, based on an analytical description of the phenomenon [16]. In [17], the analytical model of an electromagnetic massive core brake actuator is based on magnetic and electric equivalent circuits of iron core, for which the lumped parameters are used for the evaluation of reluctances.

The above mentioned simplified models, in spite of the high efficiency, could be not sufficient to describe the real behaviour of the whole system in a proper way.

Consequently, the authors focused on the development of an innovative model of an Magnetic Brake System test-rig, able to couple electromagnetic, circuital and mechanical parts of the system and to achieve a good compromise between accuracy and efficiency. Another goal of this approach is the modularity. The model must be able to describe different supply circuit topology and different Magnetic Brake System test-rig layouts (characterized by a different number of brake polar expansions)[2].

The physical system is composed by three main components (see Figure 1):

- polar expansion (replicated n times);
- rail;
- electric plant (circuit).

In this paper two models are proposed: a complete 3D Partial Differential Equations (PDE) model (which reproduces the interaction among polar expansion, rail and electric plant) and a simplified one, which is a lumped parameter Ordinary Differential Equations (ODE) model extracted from the complete one. The lumped parameter model aims at further improving the compromise between accuracy and efficiency with respect to the complete one.
The main parts of the complete 3D model are the following:

- circuit model;
- rail-polar expansion electromagnetic model;
- rail-polar expansion mechanical multibody model.

On the other hand, the main parts of the lumped parameter model are the following:

- circuit model;

- simplified rail-polar expansion electromagnetic model, including:
  - inductance model;
  - force model;
- rail-polar expansion mechanical multibody model.

The PDE electromagnetic part of the complete model is implemented in *COMSOL* [18]. At each time integration step, the model is solved in steady-state conditions: this assumption is acceptable if the integration time step Δt is small enough. The other parts of the complete model (ODE parts) are implemented in *MATLAB* [19]. Instead, all the simplified model (composed only by ODE parts) is implemented in *MATLAB*.

Both the simplified and the whole model have been developed and validated in collaboration with *Italcertifer S.p.a.* (*Ferrovie dello Stato* group, owner of the Italian railway network) and compared with other models present in literature [20]. In particular, the experimental data are referred to the test-rig suitably built in the research center "Centro di Dinamica Sperimentale dell'Osmannoro" (CDSO) in Florence (Italy) for the verification of such components. The technical and physical data employed for the development of the model were provided by *Italcertifer S.p.a.*.

2. General architecture

Generally, a Magnetic Brake System is a typical mechatronic application, as shown in Figure 2, because it comprises many mechanical and electrical devices. In particular, in Figure 2 the polar expansion, the rail and the electric plant are highlighted.

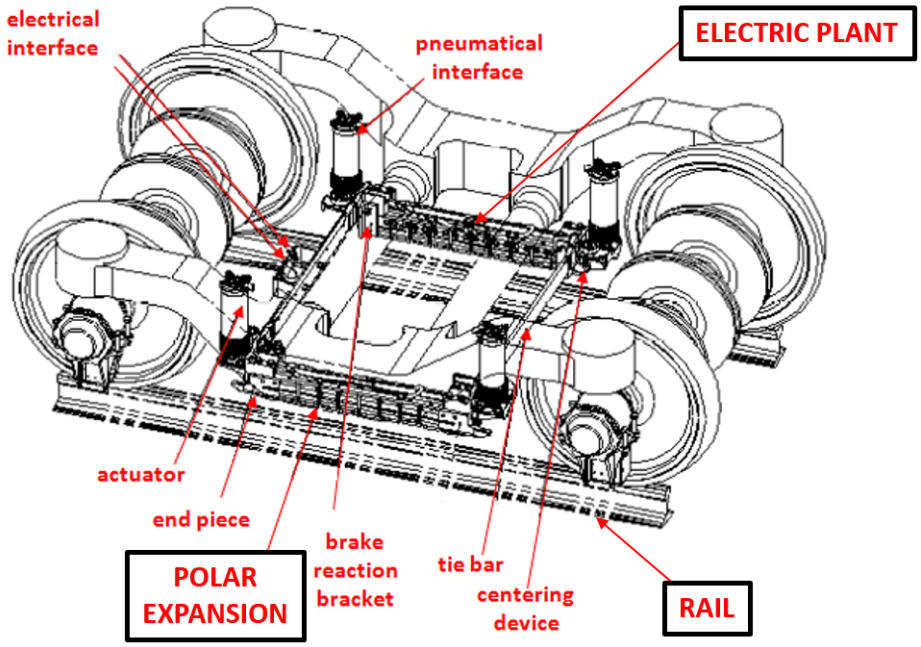

Figure 2. Main components of a magnetic braking system.

According to the introduction, the complete model shown in Figure 3 consists of the following parts:

- the circuit model solves the electric dynamics characterizing the Magnetic Brake

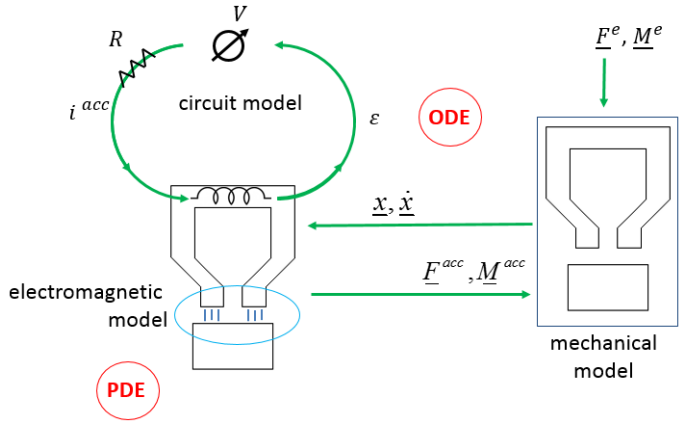

Figure 3. General architecture scheme of the complete model.

System supply system; the inputs are the voltage V and the counter electromotive force ε, while the output is the current i^{acc};

- the electromagnetic model solves the electromagnetic problem; the inputs are the current i^{acc}, the position $\underline{x} = (x\ y\ z\ \alpha\ \beta\ \gamma)^T$ and velocity (both translational and rotational) $\dot{\underline{x}} = (\dot{x}\ \dot{y}\ \dot{z}\ \dot{\alpha}\ \dot{\beta}\ \dot{\gamma})^T$ between rail and polar expansion, while the outputs are the electromagnetic force $\underline{F}^{acc}$ and moment $\underline{M}^{acc}$ and the counter electromotive force ε;
- the mechanical multibody model describes the mechanical interaction between rail and singular polar expansion; the inputs are the electromagnetic force $\underline{F}^{acc}$ and moment $\underline{M}^{acc}$ and the possible external load $\underline{F}^e$, $\underline{M}^e$ acting on it (e.g. interaction with the vehicle) and the outputs are the position $\underline{x}$ and velocity $\dot{\underline{x}}$ (between rail and polar expansion).

From the previous complete model, a simplified lumped parameter model is extracted. The aim of the new model is to achieve an accuracy comparable to the complete model one and to significantly reduce the computational time. The simplified model shown in Figure 4 consists of the following parts:

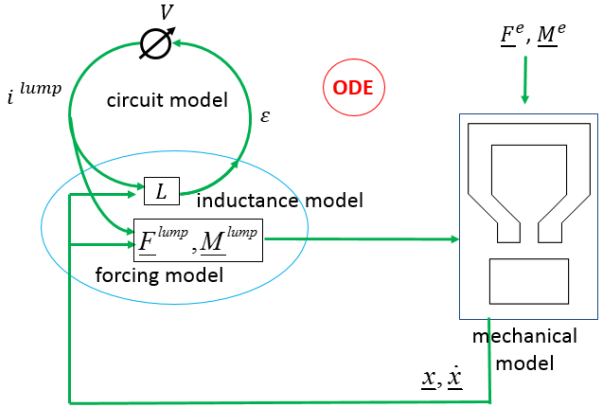

Figure 4. General architecture scheme of the simplified model.

- the circuit model solves the electric dynamics characterizing the Magnetic Brake System supply system; the inputs are the voltage V and the counter electromotive force ε, while the output is the current i^{lump};
- the simplified electromagnetic model is composed by the two sub-models (approximating the real electromagnetic model):

- the inductance model computes the approximated inductance value; its inputs are the current i^{lump}, the relative position $\underline{x}$ and velocity $\underline{\dot{x}}$ while the output is defined by the counter electromotive force ε;
- the force model calculates the approximated electromagnetic forces and moments exerted by the Magnetic Brake System; the inputs are the current i^{lump}, the relative position $\underline{x}$ and velocity $\underline{\dot{x}}$ while the outputs are the force $\underline{F}^{lump}$, moment $\underline{M}^{lump}$;

- the mechanical multibody model describes the mechanical interaction between rail and singular polar expansion; the inputs are the electromagnetic force $\underline{F}^{lump}$, moment $\underline{M}^{lump}$ and the possible external load $\underline{F}^{e}$, $\underline{M}^{e}$ acting on it (e.g. interaction with vehicle) and the outputs are the relative position $\underline{x}$ and velocity $\underline{\dot{x}}$.

An important feature of the developed architecture is the modularity of the approach. The singular polar expansion model can be repeated n times (where n represents the polar expansions number), allowing the simulation of different Magnetic Brake System layouts by adding or reducing the polar expansions number. In this study case 10 poles are implemented, even if this number can be different for other Magnetic Braking Systems.

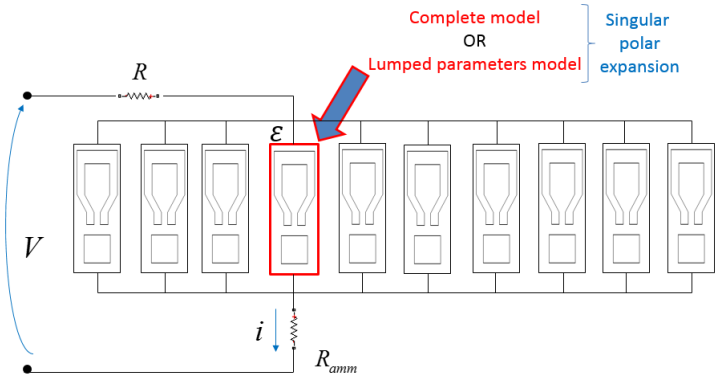

Figure 5. General architecture scheme of the whole model.

In the complete model, as shown in Figure 6, to integrate the electromagnetic, the circuital and the mechanical parts, the model numerical architecture is divided into two parts:

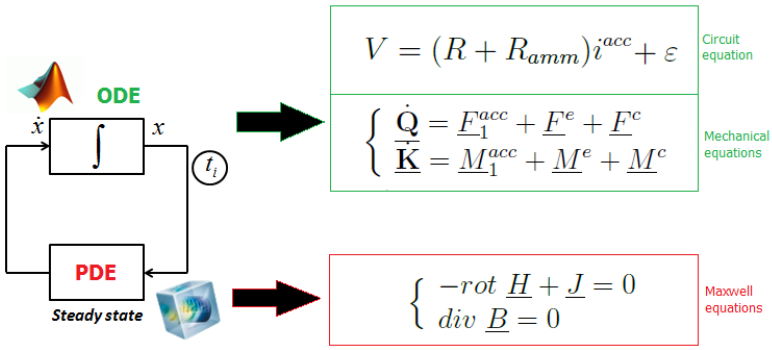

Figure 6. Numerical flowchart of the proposed algorithm.

- Partial Differential Equations (PDE) problem: the Maxwell equation for the electromagnetic model is solved in steady-state conditions using the *COMSOL* software.

- Ordinary Differential Equations (ODE) problem: both the motion equations of the mechanical model and the equations of the circuit model are solved in *MATLAB*.

This approach separately describes the electromagnetic part and the electric/mechanic ones, reaching a good trade off between numerical efficiency and accuracy. Such decoupling is possible if the time integration step Δt is small enough; under this assumption, within the temporal interval Δt, the electromagnetic problem is solved as steady-state (according to Maxwell equation).

An implicit, variable order and variable step ODE-solver is used to simulate the time-dependent part, suitable for stiff problems (conventionally defined as *ode15s*)[23], [24].

The electromagnetic model is simulated using an iterative non linear solver based on inexact Newton methods [22]. The linear problems arising from the non linear solver are solved through an iterative method (*BicGStab* [25]). The previously mentioned algorithms have been chosen in order to obtain the best trade off between numerical efficiency and accuracy.

As regards the mesh, for the electromagnetic problem, it has been realized by means of threedimensional BRICK elements, to obtain acceptable efficiency performances and accurate results [29].

Conversely, since the simplified model is completely composed by Ordinary Differential Equations, it is entirely solved with the ODE-solver *ode 45*, realizing the best compromise between accuracy and efficiency.

3. Model description

In the following sections the three sub-models of the complete model and the four sub-models of the simplified lumped parameter model will be described in detail. In particular, the Magnetic Brake System model evaluates the temporal evolution of the following variables:

- electric current i of the electrical plant and all the circuital variables;
- electromagnetic force $\underline{F}$ and moment $\underline{M}$ acting on the rail;
- the relative position $\underline{x}$ and velocity $\underline{\dot{x}}$ between polar expansion and rail.

3.1. *Complete model*

The complete model reproduces the electromagnetic, the circuital and the mechanical parts of the system.

3.1.1. Circuit model

This section describes the main features of the whole electric circuit. The input are the voltage V, and the counter electromotive force ε (provided by the rail-polar expansion electromagnetic model).

This component, which is represented in Figure 7, consists of an horseshoe shaped electromagnet and a block of ferromagnetic material. An electromagnet winding consists of N turns of insulated conductive material (e.g. copper). The system variables are the electric current i^{acc} and the air gap amplitude x, while A_1 and A_2 are respectively the surfaces of the rail fraction and of a single side of the polar expansion (see Figure 7). The relationships between V and i^{acc} can be written as follows:

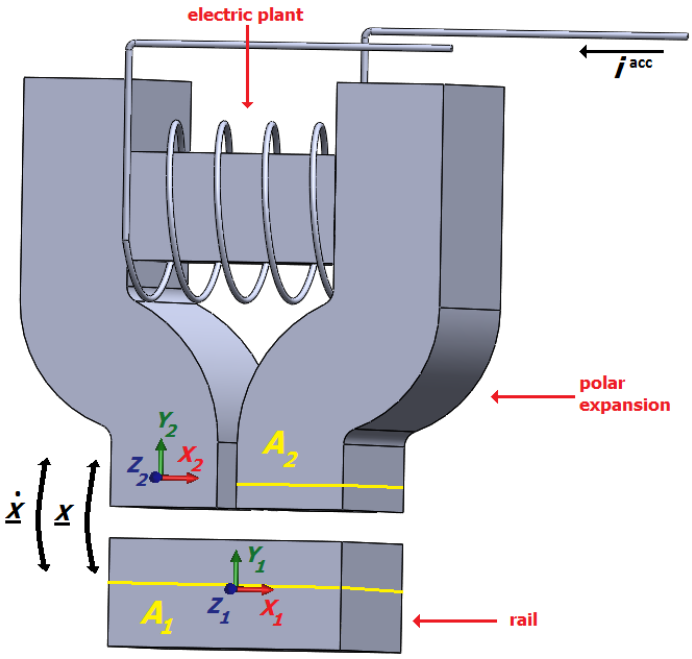

Figure 7. Simple magnetic actuator model.

$$V = (R + R_{amm})i^{acc} + \varepsilon, \tag{1}$$

where R is the winding equivalent resistance and R_{amm} is the ammeter resistance. In particular, the counter electromotive force ε is defined as:

$$\begin{aligned} \varepsilon &= \tfrac{d\Phi}{dt}, \\ \Phi &= \textstyle\int_{A_2} \underline{B} \cdot \underline{n}\, dA_2 \end{aligned} \tag{2}$$

where Φ is the magnetic flow.
The output is the current i^{acc}.

3.1.2. Electromagnetic model

The model inputs are the current i^{acc}, the relative position $\underline{x}$ and velocity $\underline{\dot{x}}$.
The geometry of the singular polar expansion is shown in in Figure 7 and is defined according to regulations prEN 16207 [26] and DIN VDE 0580 § 44 [27].
The electromagnetic model is characterized of the magnetic field $\underline{H}$, the current density $\underline{J}$ and the magnetic induction $\underline{B}$. These variables are combined according to the Maxwell equations:

$$\begin{cases} -rot\ \underline{H} + \underline{J} = 0 \\ div\ \underline{B} = 0 \end{cases}, \tag{3}$$

where the approximated relation between i^{acc} and $\underline{J}$ is the following:

$$\underline{J} = \frac{i^{acc}}{S}\underline{n}, \quad i^{acc} = \int_S \underline{J}\, dS, \tag{4}$$

in which S defines the wire section and $\underline{n}$ is the vector unit normal to the wire section.

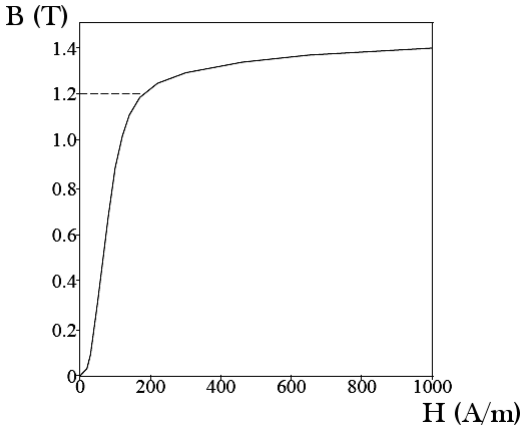

Figure 8. B-H curve for 3% silicon steel.

Using the constitutive relation $\underline{B} = \mu \underline{H}$, where $\mu = \mu_0 \mu_r$ (μ_0 andμ_r are respectively the void and relative permeability) and the saturated relation between B and H (see Figure 8), the electromagnetic forces are calculated through the Maxwell stress tensor [28]:

$$T = -\frac{1}{2}\left(\underline{H} \cdot \underline{B}^T + \underline{B} \cdot \underline{H}^T\right) \tag{5}$$

More in detail, the forces and moments acting on the polar expansion and on the rail are calculated according to the surface integral Equations (6) and (7):

$$\underline{F}_1^{acc} = \int_{A_1} T\underline{n}_1 \, dA_1, \quad \underline{F}_2^{acc} = \int_{A_2} T\underline{n}_2 \, dA_2, \tag{6}$$

$$\underline{M}_1^{acc} = \int_{A_1} \underline{r}_1 \times (T\underline{n}_1) \; dA_1, \quad \underline{M}_2^{acc} = \int_{A_2} \underline{r}_2 \times (T\underline{n}_2) \; dA_2, \tag{7}$$

where $\underline{n}_1$ and $\underline{n}_2$ are the outward normals respectively from the polar expansion and the rail, $\underline{r}_1$ and $\underline{r}_2$ are the distances from the center of mass of polar expansion and rail, A_1 and A_2 are the surfaces of rail and polar expansion that the forces $\underline{F}_1$ and $\underline{F}_2$ respectively act on (see Figure 7).

The outputs are the electromagnetic force $\underline{F}_1^{acc}$, moment $\underline{M}_1^{acc}$ acting on the rail and the counter electromotive force $\varepsilon = \frac{d\Phi}{dt}$.

3.1.3. Mechanical model

The mechanical model defines the motion equation of the polar expansion. The inputs are defined by the electromagnetic forces $\underline{F}_1^{acc}$, the moments $\underline{M}_1^{acc}$ and the possible external load $\underline{F}^e$, $\underline{M}^e$ acting on it (e.g caused by the train).

The model is able to describe the motion considering all the 6 DOF ($\underline{x} = (x \; y \; z \; \alpha \; \beta \; \gamma)^T$) of the polar expansion and therefore will be characterized by the following equation:

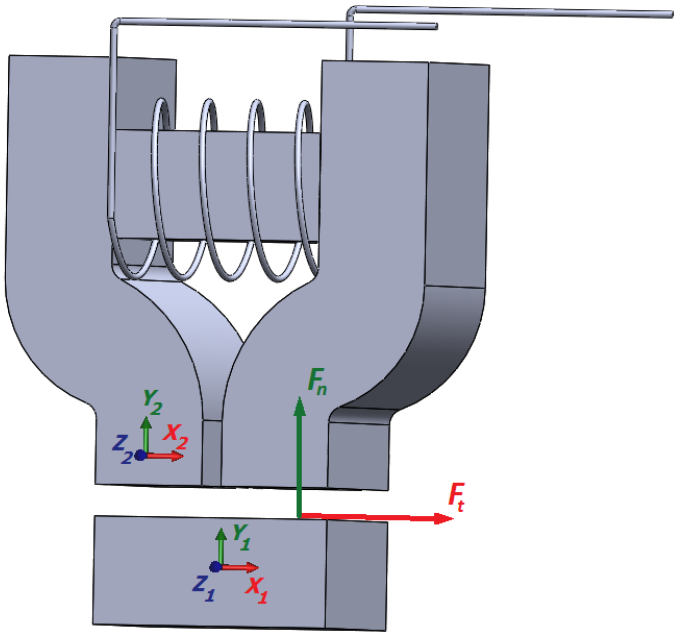

Figure 9. Simple magnetic actuator model.

$$\begin{cases} \dot{\underline{\mathbf{Q}}}_1 = \underline{F}_1^{acc} + \underline{F}^e + \underline{F}_1^c \\ \dot{\underline{\mathbf{K}}}_1 = \underline{M}_1^{acc} + \underline{M}^e + \underline{M}_1^c \end{cases} \tag{8}$$

where $\underline{\mathbf{Q}}_1$ and $\underline{\mathbf{K}}_1$ are respectively the linear moment and the moment of the linear moment of the polar expansion, $\underline{F}_1^c$ and $\underline{M}_1^c$ are the force and moment given by the train. The Equation (9) defines the force contact vector:

$$\underline{F}_1^c = \begin{pmatrix} F_t \\ F_n \\ 0 \end{pmatrix} = \begin{pmatrix} f(s) \cdot F_n \\ Kd + c\dot{d} \\ 0 \end{pmatrix}, \tag{9}$$

where d is the penetration between polar expansion and rail surface and $f(s)$ is the friction coefficient [31], [30], [32], [33]. In particular [21], s represents the sliding between rail and polar expansion, which determines the friction coefficient, as shown in Figure 10.

The moment contact vector is expressed by following equation:

$$\underline{M}_1^c = (\underline{P}_c - \underline{O}_1) \times \underline{F}_1^c, \tag{10}$$

where $\underline{P}_c$ is the contact point position and $\underline{O}_1$ is the center of mass of the polar expansion.

The outputs are represented by the relative position $\underline{x} = (x\ y\ z\ \alpha\ \beta\ \gamma)^T$ and the velocity $\dot{\underline{x}} = (\dot{x}\ \dot{y}\ \dot{z}\ \dot{\alpha}\ \dot{\beta}\ \dot{\gamma})^T$.

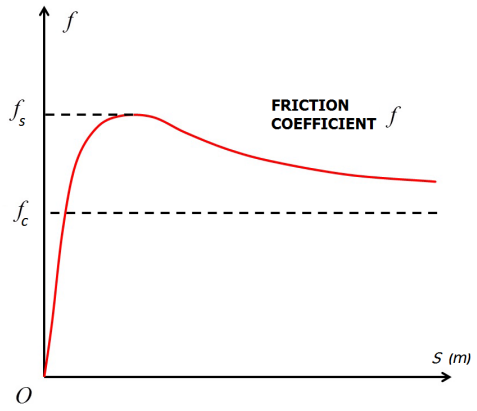

Figure 10. Friction coefficient f behaviour in function of the sliding s.

3.2. *Lumped parameter model*

The simplified model is extracted from the previous one. The lumped parameter model allows to improve the compromise between accuracy and efficiency provided by the complete one. In parallel with the complete model, it is divided into:

- circuit model;
- simplified electromagnetic model:
  - inductance model;
  - forcing model;
- mechanical model.

This model will be compared with the complete one in section 5.

3.2.1. Circuit model

The input are the voltage V and the counter electromotive force ε. The relationships between V and i^{lump}, is the following:

$$V = (R + R_{amm})i^{lump} + \varepsilon, \tag{11}$$

where, in this case, differently from the Equation (1), $\varepsilon = \frac{d\Phi(\underline{x})}{dt} = \frac{d(L(\underline{x})i^{lump})}{dt}$ and

$$\frac{d\Phi}{dt} = \frac{dL}{dt}i^{lump} + L\frac{di^{lump}}{dt} = \frac{dL(\underline{x})}{d\underline{x}} \cdot \dot{\underline{x}}i^{lump} + L\frac{di^{lump}}{dt}. \tag{12}$$

The output of this model is the current i^{lump}.

At this point, for simplicity, the inductance function $L(\underline{x})$ can be computed defining a range of possible positions ($\underline{x} \in \Omega_x$) to which the corresponding inductance values (computed with the Maxwell equations) are associated, and hence defining a multidimensional Look-Up Table (see Section 3.2.2). If the Look-Up Table is simple enough, an analytical approximation of the Look-Up Table is also possible.

3.2.2. Inductance model

The inductance model computes the inductance function $L(\underline{x})$ value for any $\underline{x}$; its inputs are the current i^{lump} and the relative position $\underline{x}$.

The inductance $L(\underline{x})$ values are extracted from the complete model according to the following algorithm:

- for each position $\underline{x} \in \Omega_x$, the magnetic field density $\underline{B}(\underline{x})$ is obtained through the Maxwell equations by the complete model;
- from Equation 2 the magnetic flow $\Phi(\underline{x})$ is calculated;
- finally, the inductance values $L(\underline{x})$ are given by $L(\underline{x}) = \Phi(\underline{x})/i^{lump}$ (i^{lump} is calculated by the complete model).

This approach allows, for any $\underline{x}$, to define the Look-Up Table of L($\underline{x}$). If the Look-Up Table is simple enough, an analytical approximation of the Look-Up Table is also possible.
The output is defined by the approximated inductance $L(\underline{x})$.

3.2.3. Forcing model

The model inputs are the current i^{lump} and the relative position $\underline{x}$.
Usually the magnetic energy U stored in an inductor is defined as:

$$U = \frac{1}{2} L (i^{lump})^2, \tag{13}$$

then, the magnetic energy U variation respect to distance $\underline{x}$ defines the electromagnetic force and moment obtained from the inductance function value, obtained in section 3.2.2:

$$\begin{pmatrix} \underline{F}_1^{lump} \\ \underline{M}_1^{lump} \end{pmatrix} = \left(\frac{dU(\underline{x})}{d\underline{x}} \right)^T = \left(\frac{d1/2L(\underline{x})(i^{lump})^2}{d\underline{x}} \right)^T = \frac{1}{2} \left(\frac{dL(\underline{x})}{d\underline{x}} \right)^T (i^{lump})^2, \tag{14}$$

The outputs are the approximated force $\underline{F}_1^{lump}$ and the approximate moment $\underline{M}_1^{lump}$.

3.2.4. Mechanical model

The mechanical model is equal to that described in section 3.1.3.

3.3. *Numerical implementation*

As already shown in Figure 6, the authors divided the numerical problem solution (of the complete model) into two parts:

- Partial Differential Equation (PDE) problem, for the electromagnetic model (solved in steady state condition within the time integration step Δt).
- Ordinary Differential Equation (ODE) problem, for the circuit and mechanical models (time-dependent).

The PDE problem part, shown in detail in Figure 11, is solved in COMSOL through an *inexact Newton's Method*, which is usually employed in sparse problems of great dimensions. The linear problems arising from the nonlinear solver are solved through an iterative method, the *BiCGStab* (BiConjugate Gradient Stabilized) [25].

The mesh has been built using three-dimensional BRICK elements, in order to maintain acceptable performances (in terms of numerical efficiency) and accurate results.

In MATLAB, the ODE problem is solved through the *ode15s* algorithm (Figure 11): this algorithm has been chosen in order to obtain the best compromise between

Table 1. Solver, tolerances and mesh features.

PDE problem (steady state):	
Newton:	
Maximum iterations number for the iterative solver	4
Relative tolerance of the iterative solver	$2.5 \cdot 10^{-6}$
BiCGStab:	
Maximum iterations number for the iterative solver	10
Relative tolerance of the iterative solver	$2.5 \cdot 10^{-6}$
Mesh:	
Minimum element size	0.000304 (m)
Maximum element size	0.00169 (m)
Maximum element growth rate	1.3
ODE problem (in Δt):	
ode15s:	
Minimum integration step-size	0.1
Relative tolerance of the integrator	10^{-3}
Absolute tolerance of the integrator	10^{-4}

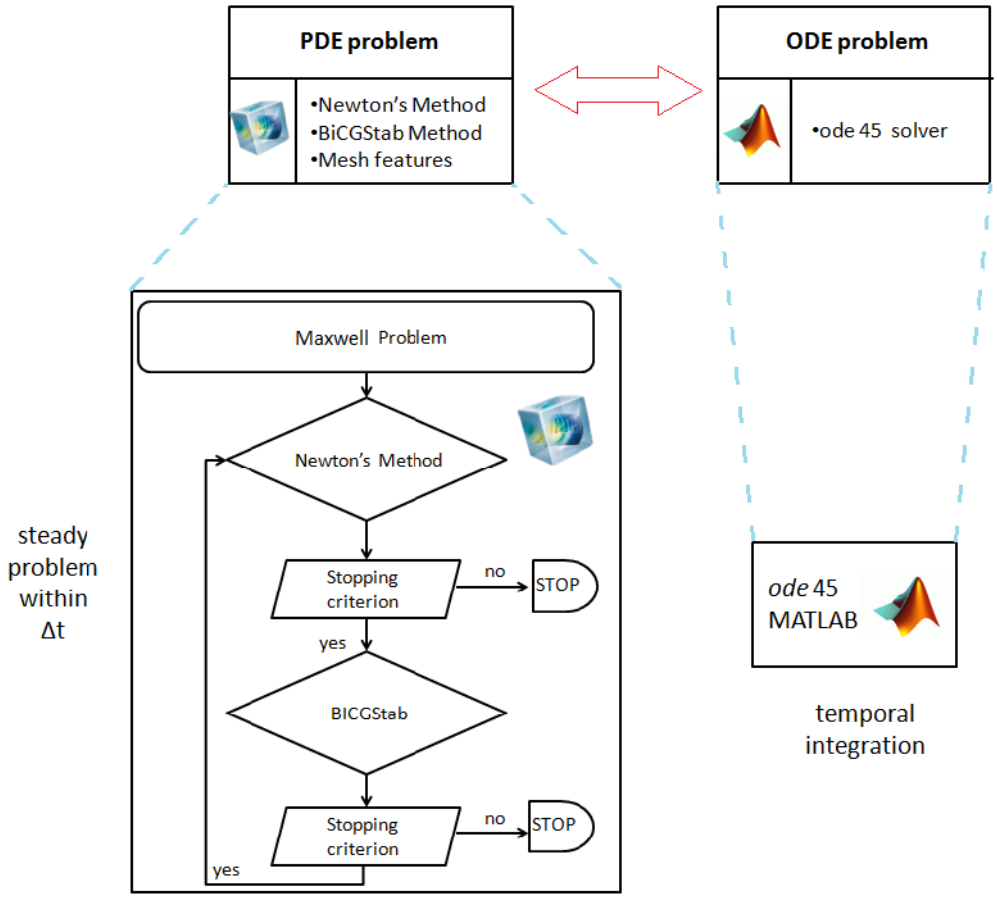

Figure 11. Numerical flowchart of the solution algorithm.

efficiency and accuracy.

The lumped parameter model is completely solved in *MATLAB* (being composed exclusively of Ordinary Differential Equations).

Solvers, tolerances and mesh features are shown in Table 1.

4. Experimental tests

4.1. *Experimental conditions*

At this initial phase of the research activity, the range of possible positions considers only one direction of motion ($\underline{x} = (0\ y\ 0\ 0\ 0\ 0)^T$), that is the normal problem. The range of the position Ω_x is from the contact between polar expansion and rail fraction ($y_1 = 0\ m$) to a relative position in which the magnetic field is dispersed in the air ($y_2 = 0.35\ m$).

Consequently, the inductance Look-Up Table $L(\underline{x})$ is reduced to a one-dimensional Look-Up Table $L^{lump}(y)$ that the authors decided to analytically approximate with the following equation:

$$L^{lump}(y) = \frac{\mu N^2 A_g}{l + y_2 \left(\frac{y}{y_2}\right)^{\alpha}}, \tag{15}$$

where α is a parameter greater than 1 (if $\alpha = 1$, the same formula present in literature is obtained, see Equation (18)). The authors suggest a range of α equal to $[3.4 - 3.6]$, for the best fitting of the real inductance value.

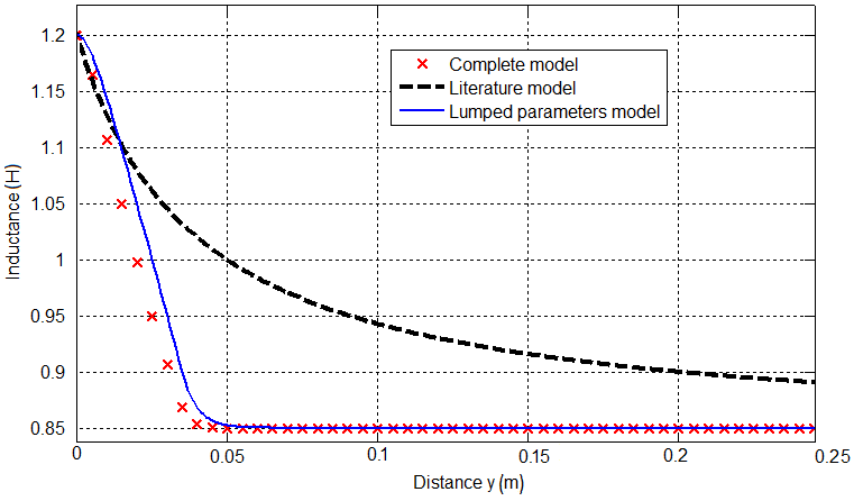

Figure 12. Inductance variation.

In Figure 12, the black dashed line represents the relation $L^{id}(y)$ usually employed in literature (see Equation 18), the red crosses line regards the inductance value calculated according to the Look-Up Table approach (see section 3.2.2) and the blue line represents the inductance computed with the Equation (15). The complete model is more accurate if compared to the lumped parameter and literature model Experimental results directly related to the inductance were not available; however, the comparison can be made considering the behaviour of the currents with respect to measured data (Figure 16).

With regard to the electromagnetic force and moment the Equation (14) becomes (in the considered simplified case):

$$\begin{pmatrix} \underline{F}_1^{lump} \\ \underline{M}_1^{lump} \end{pmatrix} = \begin{pmatrix} 0 \\ \frac{1}{2}\frac{dL^{lump}(y)}{dy}(i^{lump})^2 \\ 0 \\ 0 \\ 0 \\ 0 \end{pmatrix}. \tag{16}$$

4.2. *Experimental data description*

The test rig is composed by ten polar expansion (the proposed model allows, however, a variable polar expansion number). The applied external forces are:

$$\begin{pmatrix} \underline{F}^e \\ \underline{M}^e \end{pmatrix} = (0\ F_y^e\ 0\ 0\ 0\ 0)^T. \tag{17}$$

The authors use a incremental F_y^e (that is put to zero after the detachment thanks to the force control system of the test rig) and measure i^{meas}, F_{y1}^{meas} (to be compared to F_{y1}^{acc} and F_{y1}^{lump} provided by the complete and simplified models respectively) and y^{meas} during all the test. The Magnetic Braking System model has been validated through comparison with experimental data provided by *Italcertifer S.p.a.* and coming from the Magnetic Brake System testing, represented in Figure 13, built at the "Centro di Dinamica Sperimentale dell'Osmannoro" (CDSO) of Florence (Italy).

The test-rig is designed in order to verify the performances in braking phase of the Magnetic Brake System, in accordance with the normative DIN VDE 0580 §44 [27]. It performs generic motions ($\underline{x}$, $\underline{\dot{x}}$) between polar expansion and rail fraction (for simplicity, at this initial phase only the normal motion along y is considered, see section 4.1).

The test-rig represented in Figure 13 comprises the following units:

- electric plant:
  - electrical components;
  - supply system;
  - current sensor;
- polar expansion:
  - polar expansion elements;
  - supports;
  - double-acting pneumatic cylinders;
  - bracket for lifting / lowering pad;
  - load cell;
- rail:
  - pneumatic cylinder;
  - rail fraction.

In particular, the rail unit is constituted by two test half rails, type UIC 60, 72 mm wide. The main parameters characterizing the electromagnetic circuit of the test-rig are shown in Table 2.

The test-rig allows the measurement of the detachment force $\underline{F}_1^{meas}$ and moment $\underline{M}_1^{meas}$ (in the considered case only F_{y1}^{meas}) to be compared to F_1^{acc}, M_1^{acc} and F_1^{lump}, M_1^{lump} provided by the complete and simplified models respectively, and of

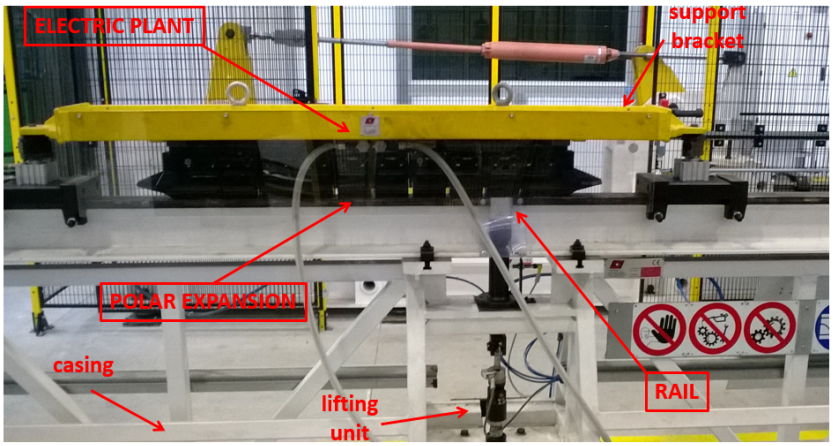

(a) Complete test rig.

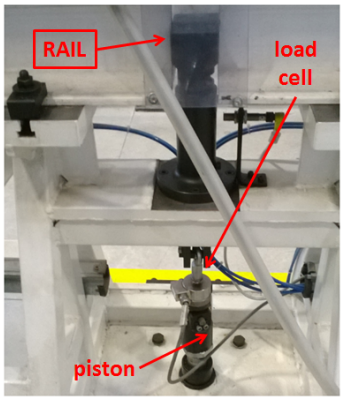

(b) Detail of the actuation system.

Figure 13. Magnetic Braking System test rig.

the displacements $\underline{x}$ (in the considered case only y^{meas}) on any type of Magnetic Braking System, and the relief of the excitation current i^{meas} of winding.

In particular, i^{meas} is measured with an ammeter situated downstream the parallel of the ten polar expansions, F_{y1}^{meas} is evaluated through a load cell placed on the pneumatic piston and y^{meas} is function of the motion of the pneumatic cylinder. The extracted experimental data refer to the full test-rig (with 10 polar expansions).

In Figures 14 and 15 the behaviour of the experimental force $F_{y1}^{meas}(t)$ and current $i^{meas}(t)$ are represented. The presence of two peaks in Figure 14 and 15 indicates that two consecutive detachment were carried out.

In the current and force behaviour modest fluctuations (see Figures 16 and 17) can be noticed (in the force behaviour this fluctuations are smaller), due to heat loss phenomena, noise and unmodelled dynamics.

The current and force peaks occur when the rail fraction is detached from the polar expansion, otherwise, in contact phase, the current remains almost constant and the force equal to zero. The authors focus primarily on the detachment phase (see Figure 16 and 17). The present study considers an interval of 0.35 seconds, which is sufficient to properly analyze the trend of the current and of the force during the detachment phase.

In Figure 16 the ideal current curve i^{id} is obtained through the following formula usually employed in the simplified literature models [20], which was implemented in the lumped parameter model instead of the Equation 15:

Table 2. Main parameters of the Magnetic Braking System.

	Polar expansion:	
A_g	0.0037 m^2	air gap section
l	0.385 m	length of the magnetic circuit
μ_r	100	relative magnetic permeability
	Rail:	
section		double-T beam
type		UIC 60
wide	72 mm	rail width
	Electric plant:	
N	95	turns number
R	4.5 Ω	resistance of a singular pad
R_{amm}	0.125 Ω	resistance of the ammeter
L	1.2 H	inductance of a singular pad
V	24 V	generator voltage
μ_0	$4\pi \cdot 10^{-7}$ H/m	void magnetic permeability
i_{sat}	100 A	saturation current
B_{sat}	1.6 T	saturation magnetic field density

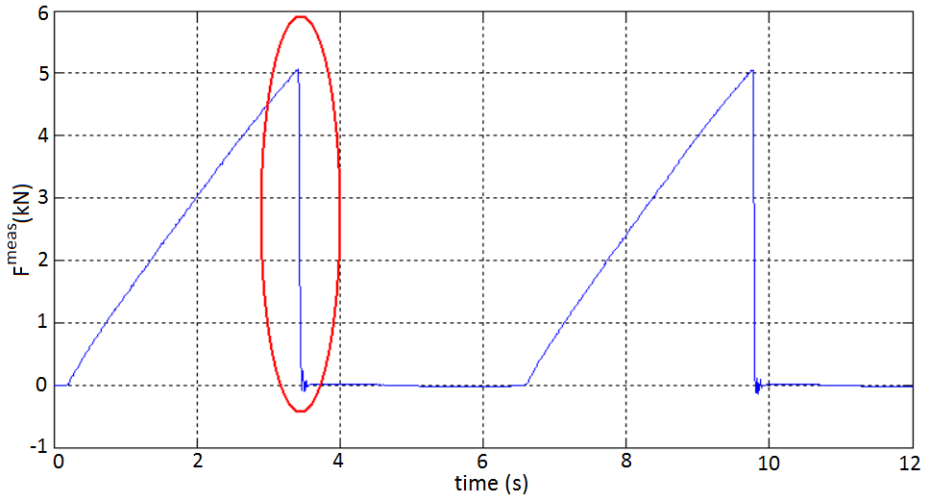

Figure 14. Behaviour of the experimental force F_{y1}^{meas} during the detachment and contact phases.

$$L^{id}(y) = \frac{\mu N^2 A_g}{l + y}. \tag{18}$$

In parallel with the previous considerations, in Figure 17 the ideal force curve F^{id} is obtained through the following formula usually employed in the simplified literature models [20]:

$$F_{y1}^{id}(y) = \frac{\mu_0 N^2 A_g (i^{id})^2}{(l + y)^2}. \tag{19}$$

In Figure 16 and 17 it can be noticed that a good matching between experimental data and the formula present in literature is not achieved (there are excessive

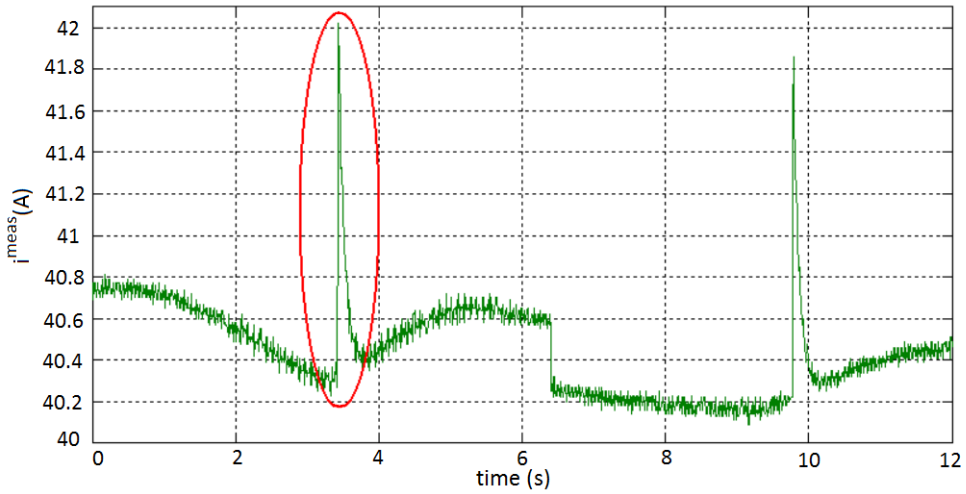

Figure 15. Behaviour of the experimental current i^{meas} during the detachment and contact phases.

delay in the detachment phase).

5. Validation and results

In this section, the authors compare simulated and experimental data referred to a Magnetic Brake System. In particular the following results are presented:

- comparison between the currents i^{lump}, i^{acc}, i^{meas} and i^{id} respectively computed in the lumped parameter and complete models, measured in the test-rig and calculated with literature equations;
- comparison between the forces $F_y^{e,lump}$, $F_y^{e,acc}$, $F_y^{e,meas}$ and $F_y^{e,id}$ respectively computed in the lumped parameter and complete models, measured in the test-rig and calculated with literature equations;
- computation time.

5.1. *Current results*

In Figure 16 i^{lump} and i^{acc}, obtained from the simulations performed with the proposed model, are compared to i^{meas} and i^{id}. The ideal current curve i^{id} is obtained considering the ideal inductance formula expressed in Equation 18 implemented in the lumped parameter model.

In particular, the time instants in which the peak values of current occur are very similar for i^{lump}, i^{acc} and i^{meas}. In addition, as in the i^{meas} curve, the growth rates of i^{lump} and i^{acc} are almost vertical, while in i^{id} the current grows more slowly. Finally, in the descent phase, the behaviour of i^{lump} and i^{acc} reproduce with a good approximation the curve i^{meas} while i^{id} is slower. The errors introduced by the new models are probably due to unmodelled dynamics. The fluctuations in i^{meas} are not reproduced by i^{id}, i^{lump} and i^{acc} behaviours because the heat loss phenomena and noise are neglected. The difference between i^{meas} and i^{id}, i^{lump} and i^{acc} in the time range between 3 and 3.4 s is due to the progressive heating of the electric circuit. This behaviour is explained in Figure 15, where in the time range between 0 and 3.4 s the current decreases (the resistance grows because of the increasing temperature).

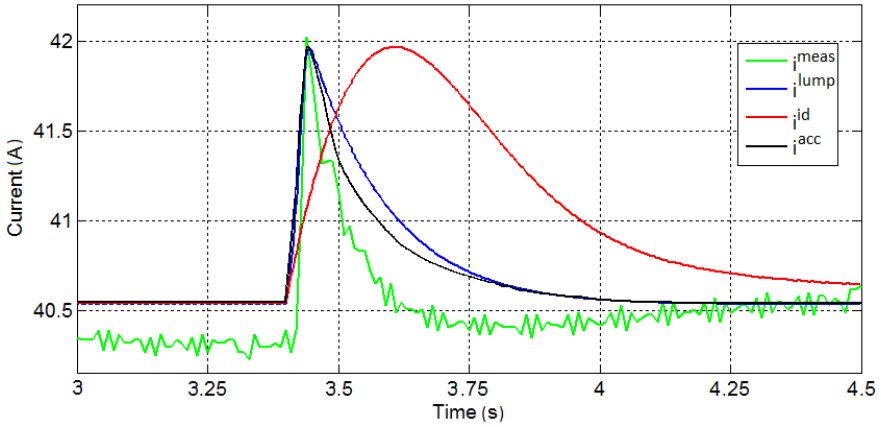

Figure 16. Comparison between i^{lump} and i^{acc}, and between i^{meas} and i^{id} in the detachment phase.

5.2. *Force results*

In Figure 17, the forces $F_y^{e,lump}$ and $F_y^{e,acc}$ obtained from the simulations performed with the proposed models are compared to the experimental force $F_y^{e,meas}$ and the ideal force $F_y^{e,id}$. The ideal force curve $F_y^{e,id}$ is obtained applying the Equation 19 in which the ideal current i^{id} behaviour is obtained considering the lumped parameter model.

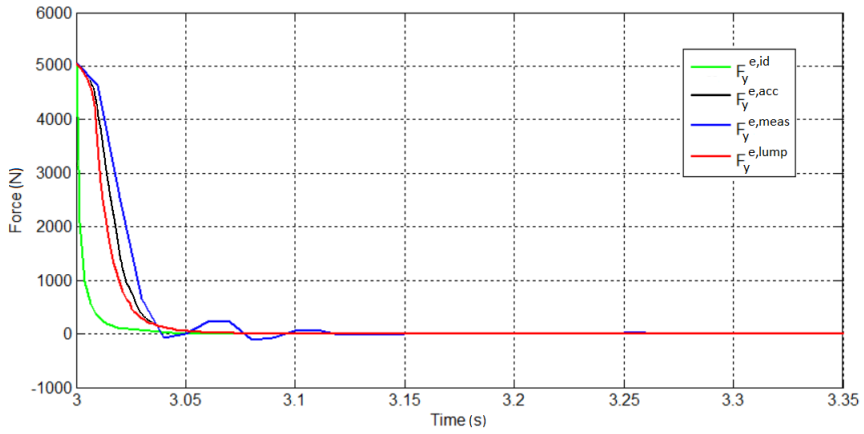

Figure 17. Comparison between the forces F_{y1}^{lump} and F_{y1}^{acc}, the experimental force F_{y1}^{meas} and the ideal force F_{y1}^{id} in the detachment phase.

In particular, the time instants in which the peak values of force occur are very similar for $F_y^{e,lump}$, $F_y^{e,acc}$ and $F_y^{e,meas}$. Finally, in the descent phase, the behaviour of $F_y^{e,lump}$ and $F_y^{e,acc}$ reproduces with a good approximation the curve $F_y^{e,meas}$ while $F_y^{e,id}$ descends more quickly. The error introduced by the new models are probably due to noise, unmodelled dynamics and heat loss. Instead, the ideal curve $F_y^{e,id}$ appears more distant from the $F_y^{e,meas}$.

In addition, among all the possible outcomes extracted from the model, the authors represent below the magnetic field density lines of $\underline{B}$ that are generated during the simulation before the detachment, at the instant $t = 3.025\ s$ (hence in the detachment phase):

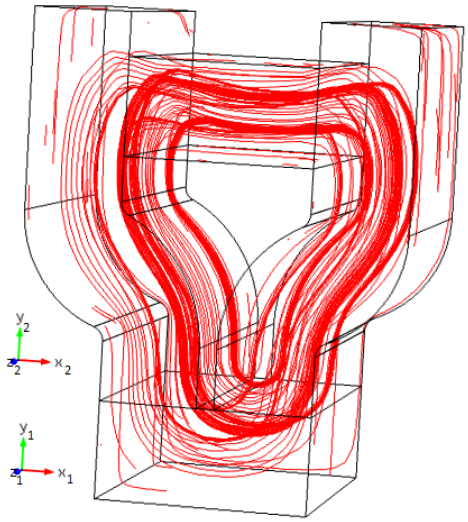

Figure 18. Magnetic field density $\underline{B}$.

5.3. *Computation time*

The singular polar expansion has been discretized using 1588 three dimensional BRICK elements with the number of DOFs equal to 2373. The simulations are performed using a standard personal computer, characterized by an Intel CORE i5 (whose clock frequency is 2.30 GHz) and by 4 Gb of RAM memory, while the installed Operative System is Windows 7 (64 bit version).

The time ratios of the machine calculation times with respect to the simulated ones are respectively 32 and 2.6 for the complete and simplified models. In particular, these results show the execution efficiency of the simplified model considering a mid range hardware employed for the simulations.

6. Conclusions and future developments

In the present paper, Magnetic Braking Systems (Magnetic Brake System) are analyzed in detail because they are widely used in railway field and deeply affect both the vehicle dynamics and the supply system behaviour.

Therefore, authors focused on the development of two models representing the electrical and mechanical behaviour of the Magnetic Brake Systems. In particular, these models consider all the electromagnetic, circuital and mechanical parts at the same time, with the purpose to obtain a complete description of the system.

Consequently, an innovative model for the simulation of the behaviour of Magnetic Braking Systems is presented with the aim of achieving a good compromise between accuracy and efficiency. In addition, the model provides a wide flexibility in terms of supply circuit topology and implementable polar expansions number (modularity). To achieve a good compromise between accuracy and efficiency and to realize a modular model, are both necessary to describe complex systems.

The results in term of currents and forces i^{acc}, i^{lump}, $F_y^{e,acc}$, $F_y^{e,lump}$ calculated with the proposed models are quite encouraging, as they show a better agreement, if compared with the measured experimental quantities i^{meas} and $F_y^{e,meas}$, with respect to variables i^{id} and F^{id} obtained considering the models commonly available in literature. Instead, the computational times are comparable.

The following future developments are scheduled for the future to improve the model accuracy:

- extension of the approach to generic motion $\underline{x}$, using generic external force $\underline{F}^e$ and moment $\underline{M}^e$ (implementation of the tangential contact problem), always considering the proposed Look-Up Table/Analytical approach;
- further experimental validations;
- simulation and validation on a real vehicle in motion;
- opportunity to consider the phenomena of heat loss (important to accurately model the current);
- more realistic features in the circuit model (mutual inductance between the coils, supply voltage variations,. . .).

Acknowledgments

Authors wish to thank *Italcertifer S.p.a.* (FS group) for cooperating to this project and for providing the technical and experimental data needed for the model development and validation.

References

[1] Jirout M, Mack W, Lugner P. Non-smooth dynamics of a magnetic track brake. *Regular and Chaotic Dynamics*. 2009; 14(6):673-681.
[2] Railway applications - braking - functional and performance criteria of electromagnetic track brake systems for use in railway rolling stock. EUROPEAN COMMITTEE FOR STANDARDIZATION. November 2010.
[3] Gfatter G, Haas S, Vohla G. Track brakes handbook. Knorr-Bremse GmbH. 2004.
[4] *Technical specification for interoperability relating to the rolling stock subsystem of the trans-European high-speed rail system*. Referred to in Article 6(1) of Council Directive 96/48/EC. 30 May 2002.
[5] Piechowiak T. Pneumatic train brake simulation method. Veh Syst Dyn. 2009; 47(12):1473-1492.
[6] David B, Haley D, Nikandros G. Calculating train braking distance. Proceedings of the Sixth Australian workshop on Safety critical systems and software vol 3. Australian Computer Society, Inc.. Sydney, 2001.
[7] Cantone L, Karbstein R, Müller L, Negretti D, Tione R, Geiβler H J. Traindynamic simulation - a new approach. 8th World Congress on Railway Research. 2008.
[8] Kang C G. Analysis of the braking system of the Korean high-speed train using real-time simulations. J Mech Sci Technol. 2007;21(7):1048-1057.
[9] Wilkinson D T. Electric braking performance of multiple unit trains. Proceedings of the Institution of Mechanical Engineers, Part D. J Automob Eng. 1985;199(4):309-316.
[10] Edwards J D, Jayawant B V, Dawson W R C, Wright D T. Permanent-magnet linear eddy-current brake with a non-magnetic reaction plate. *IEE Proc-Electr. Power Appl.* 1999;146(6).
[11] Yao M, Wang L. Analysis and simulation of on the influencing factors of braking force for permanent magnetic brake. Applied Mechanics and Materials. 2013;278-280(278-281).
[12] Gay S E, Ehsani M. Analysis and experimental testing of a permanent magnet eddy-current brake. IEEE. 2005.
[13] Baran W I A. Influence of different magnetic field profiles on eddy-current braking. 2nd European Conference on Hard Magnetic Materials. 1969.
[14] Hazry D, Ahmed S F, Faizi M K. Magnetic force based absorber system - a novel approach in vibration absorption application. Wulfenia Journal. 2012;19(12).
[15] Dülk I,Kovácsházy T. Modelling of a linear proportional electromagnetic actuator and possibilities of sensorless plunger position estimation. IEEE, 12th International Carpathian Control Conference (ICCC). 2011.
[16] Gholizad H, Mirsalim M, Mirzayee M, Tsukerman I A. Motional eddy currents analysis in moving solid iron using magnetic equivalent circuits method. ACES. 2005.
[17] Vekara T T, Eriksson J T, Tanttu J T. Dynamic model of an electromagnetic massive core brake actuator. IEEE Transactions on Magnetics. 1996;32(3).
[18] Comsol Multiphysics®site:http://www.comsol.com/.
[19] Mathworks®site: https://www.mathworks.it/.
[20] Schweitzer G, Maslen E H. Magnetic bearings - theory, design and application to rotating machinery. Springer. 2009.
[21] Cheli F, Pennestr E. Kinematics and dynamics of multibody systems. 2009.
[22] Kelley C T. Solving nonlinear equations with Newton's method. No. 1 in Fundamentals of Algorithms. 2003.
[23] Bogacki P, Shampine L F. A 3(2) pair of Runge-Kutta formulas. Appl. Math. Letters. 1989;2:321-325.
[24] Dormand J R, Prince P J. A family of embedded Runge-Kutta formulae. J. Comp. Appl. Math.. 1980;6:19-26.
[25] Vorst V D. Bi-CGSTAB: A fast and smoothly converging variant of Bi-CG for the solution of non-symmetric linear systems. SIAM J. Sci. and Stat. Comput.. 1992;13(2):631-644.

[26] European standard prEN 16207 Railway applications - braking - functional and performance criteria of electromagnetic track brake systems for use in railway rolling stock. Brussels, 2010.
[27] German standard DIN VDE 0580 Electromagnetic devices and components. Berlin, 2000.
[28] Griffiths D J. Introduction to electrodynamics. Benjamin Cummings Inc.. 2008.
[29] Strang G, Fix G. An analysis of the finite element method. Englewood Cliffs. 1973.
[30] Auciello J, Meli E, Falomi S, Malvezzi M. Dynamic simulation of railway vehicles: wheel/rail contact analysis. Vehicle System Dynamics. 2009;47:867-899.
[31] Kalker J. Three-dimensional elastic bodies in rolling contact. Kluwer Academic Publishers. 1990.
[32] Meli E, Falomi S, Malvezzi M, Rindi A. Determination of wheel - rail contact points with semianalytic methods. *Multibody System Dynamics*. 2008;20(4):327-358.
[33] Spiryagin M, Cole C, Sun Y Q. Adhesion estimation and its implementation for traction control of locomotives. International Journal of Rail Transportation. 2014;2(3):187-204.